Rare Met. (2021) 40(4):952–960
https://doi.org/10.1007/s12598-020-01563-6

RARE METALS
www.editorialmanager.com/rmet

ORIGINAL ARTICLE

The microstructural evolution and wear properties of Ni60/high-aluminum bronze composite coatings with directional structure

Xiao-Tian Yang*, Xiu-Qian Li, Qiang-Bin Yang, Jun-Ling Duan, Xiao-Yue Fu, Heng-Li Wei, Wen-Sheng Li

Received: 22 September 2019 / Revised: 2 December 2019 / Accepted: 4 August 2020 / Published online: 31 August 2020

Abstract The directional structure of Ni60/high-aluminum bronze composite coating was formed using induction remelting and forced cooling. The microstructural evolution and the characteristics of interface growth were studied. The results showed that the remelted coating formed metallurgical bonding with the substrate. The microstructures changed from plane crystal to dendrite, cellular dendrite, fine cellular dendrite, and then to dendrite again with the increase in the cooling rate. The crystal grew along the heat flow direction and had (111) and (200) preferred orientations when the cooling rate was 1.886 ml·min^{-1}·mm^{-2}. The plane crystal, dendrite and cellular dendrite were mainly composed of compounds and solid solutions with Ni, Fe and Cu, and they were surrounded by strengthening phases composed of Cr, C and B. The grain boundary of directional structure coatings showed the characteristic of regular eutectic growth, but grain boundary of remelted coating presented characteristic of divorced eutectic growth. The wear resistance of directional structure coatings is better than that of remelted coating.

Keywords Aluminum bronze composite coating; Induction remelting; Directional structure; Grain boundaries; Preferred orientation

1 Introduction

At present, the coatings with high hardness and wear resistance are the research hot spots in the field of surface engineering. Ni60 self-fluxing alloy powder has good processing properties, corrosion resistance, oxidation resistance and excellent wear resistance at both room and high temperatures [1–3]. Hence, it is widely used as the coating materials. However, due to complex specifications of products in industries, the single coating cannot meet the requirements of severe working conditions. To improve the coating anti-wear properties, the researchers have added various reinforcements to the matrix materials (such as CeO_2, WC, Al_2O_3 and Cu_2O) [4–7]. However, the addition of the second strengthening phase usually causes the uneven structure, the unreliable micro-interface between the strengthening phase and matrix materials, and the stress crack due to the interface micro-stress concentration [8, 9]. In order to overcome these problems, high-aluminum bronze powder which has good anti-friction properties [10, 11] was added to Ni60 alloy powder to prepare multi-component composite coatings. The result showed that two kinds of powders have good compatibility performance and

X.-T. Yang*, X.-Q. Li, J.-L. Duan, X.-Y. Fu, H.-L. Wei, W.-S. Li
College of Materials Science and Engineering, State Key Laboratory of Advanced Processing and Recycling of Nonferrous Metals, Lanzhou University of Technology, Lanzhou 730050, China
e-mail: yangxiaotian@sohu.com

X.-T. Yang
Wenzhou Engineering Institute of Pump & Valve, Lanzhou University of Technology, Wenzhou 325105, China

Q.-B. Yang
Chongqing Key Laboratory of Environmental Materials & Remediation Technologies, College of Chemistry & Environmental Engineering, Chongqing University of Arts and Sciences, Chongqing 402160, China

X.-Y. Fu
Department of Material and Chemical Engineering, College of Technology and Engineering. Lanzhou University of Technology, Lanzhou 730050, China

give full play to multi-component and multi-functional performance [12].

It has been reported that directional microstructures can control grain orientation to obtain columnar or single-crystal organization, eliminate the transverse grain boundaries and improve the longitudinal mechanical properties [13–16]. In order to further improve the fusion rate of multi-component coatings and optimize the structure, the directional structure of Ni60/high-aluminum bronze composite coating was prepared by the induction remelting and forced cooling method, and the formation characteristics and mechanism of the composite coatings were studied.

2 Experimental

2.1 Sample preparation

The S45C steel was employed as the substrate material with the size of 100 mm × 100 mm × 13 mm. The feedstock powders were self-fluxing Ni60 alloy powder and high-aluminum bronze alloy powder, and the two powders were mixed with a weight ratio of 8:2. The chemical compositions of two kinds of powders are given in Tables 1 and 2.

The substrate material was roughened by using sand-blast, and then the coatings with the thickness of ~ 0.7 mm were prefabricated by the supersonic plasma spraying system (DH-2080), with the following parameters: spraying distance of 125 mm, spraying voltage of 150 V, spraying current of 315 A and feeding voltage of 10 V. The primary gas was Ar, and the secondary gas was H_2.

The as-sprayed coating was remelted by using high-frequency induction heating equipment (SPG-30B) and then was forced-cooled by using tap water to make it form directional structure. The plane heating was adopted during the induction remelting, and the distance between the coil and the specimen surface was 3-4 mm with the heating power of 3.2 kW and the frequency of 175 kHz. The cooling rate was 0, 0.943, 1.415, 1.886 and 2.358 $ml \cdot min^{-1} \cdot mm^{-2}$, respectively.

2.2 Friction and wear testing

The friction and wear properties were tested using MMW-1A friction tester with the revolution rate 50 $r \cdot min^{-1}$ and the load of 50 and 150 N, respectively, for 10 min at room temperature. The wear resistance of coatings was evaluated by the wear weight loss of specimens using an analytical balance.

Table 1 Chemical composition of Ni60 alloy powder (wt%)

Cr	B	Si	Fe	C	Ni
15.0–17.0	3.0–4.0	3.5–5.0	0–15.0	0.6–1.2	Bal.

Table 2 Chemical composition of high-aluminum bronze powder (wt%)

Cu	Al	Mn	Fe	Co	Ni
70.0–80.0	12.0–16.0	0.5–2.0	2.0–4.0	0.2–0.5	0.2–.5

2.3 Characterization methods

The microstructure of the coatings was observed by optical microscope (OM, MEF3A). The surface morphology and worn surface morphology were studied by scanning electron microscope (SEM, QuantaFEG450). Electron probe micro-analysis (EPMA, EPMA-1600) was used to analyze the distribution of elements. The phases were analyzed by X-ray diffractometer (XRD, D/MAX2500 type PC).

3 Results and discussion

3.1 Microstructures

As presented in Fig. 1, the as-sprayed Ni60/high-aluminum bronze coating forms typical lamellar structure with the mechanical bonding at the coating interface. The microstructures consist of flattened particles, unbelted particles and defects such as oxides and pores.

The microstructures of composite coatings under induction remelting and forced cooling are shown in Fig. 2. It can be clearly observed that the white bright band formed at the interface of the induction remelting coating and all of

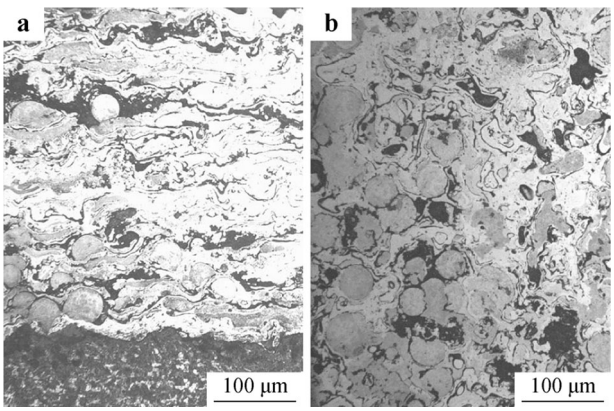

Fig. 1 OM images of as-sprayed coating: **a** cross section and **b** surface

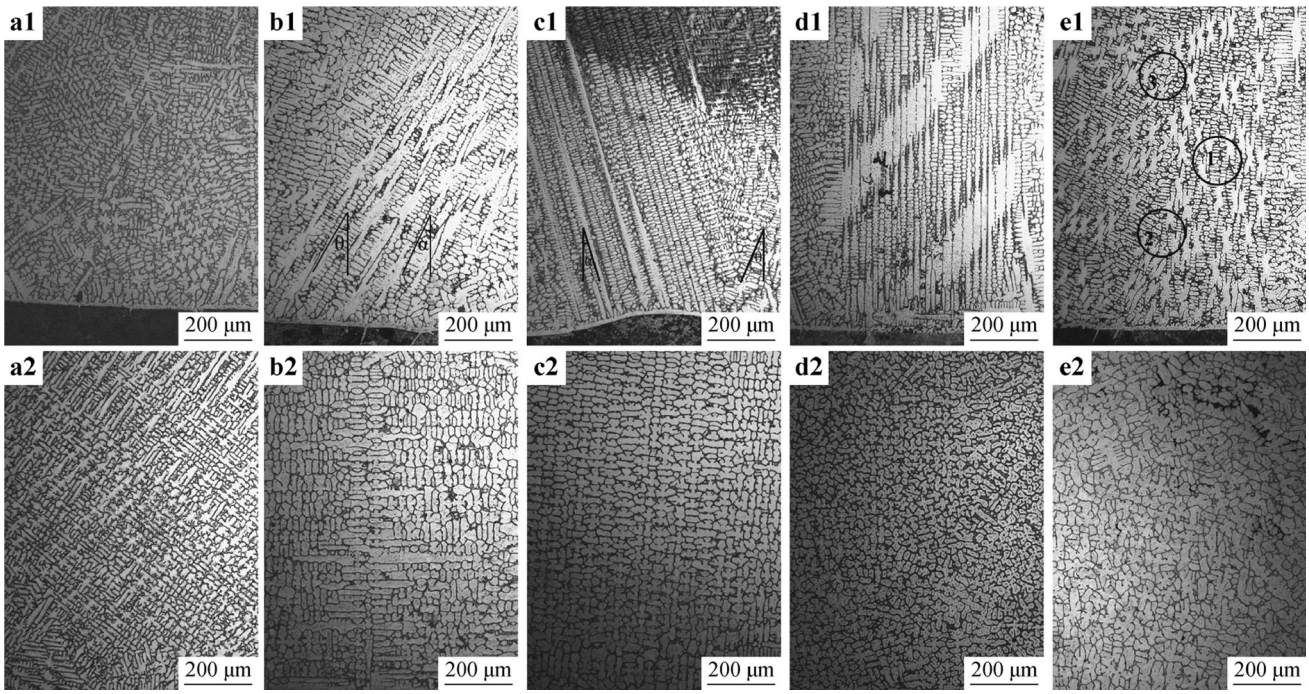

Fig. 2 OM images of coating cross section and surface under different cooling rates: **a1**, **a2** 0 ml·min^{-1}·mm^{-2}; **b1**, **b2** 0.943 ml·min^{-1}·mm^{-2}; **c1**, **c2** 1.415 ml·min^{-1}·mm^{-2}; **d1**, **d2** 1.886 ml·min^{-1}·mm^{-2}; and **e1**, **e2** 2.358 ml·min^{-1}·mm^{-2}

the coatings under different cooling rates, as shown in Fig. 2a1–e1. The element contents of the white bright band were analyzed by energy-dispersive spectroscopy (EDS), as shown in Table 3. The results show that Fe, Ni, Cr and Cu are all enriched in white bright band of both coatings. It indicates that elements of the coating and substrate under high temperature completely diffused in the remelting process, which could reduce or eliminate the cracks. The diffusion layer is obvious and the metallurgical bonding can be observed, signifying an enhanced interfacial adhesion compared with the as-sprayed coatings [17].

It also can be concluded that from EDS results the content of Fe is higher near the interface of remelted coating than that of directional structure coating due to that the skin effect [18] of the simple remelting process makes the interface maintain a higher temperature and establishes a positive temperature gradient from the interface to the coating surface, and there is a sufficient time to make elements of the substrate diffuse to the coating, but the phenomenon is obviously inhibited under the condition of forced cooling because of rapid cooling in larger temperature gradients. EPMA maps (Figs. 3, 4) present the major elemental distributions of the remelted coating and directional structure coating. Excessive Fe needs good metallurgically compatible elements to react with and reach the stable state, resulting in a negative diffusion gradient of Ni and Cu in the coating [19], as shown in Figs. 3 and 4. Therefore, it is regarded that the formation of the white bright band is a metallurgical reaction result induced and involved by substrate elements and driven by thermodynamics and dynamics.

Furthermore, during the process of the interface formation, the coating elements continue to diffuse to the interior of the substrate along the grain boundary, forming the pinning effect, as shown by the arrow pointed in Fig. 4, which would enhance the bond strength of interface. However, the coating elements strongly penetrate to the substrate in directional structure coatings, which forms the wrap-around on the substrate grains and has better pinning effect compared to the remelted coating, but the diffusion

Table 3 EDS results of metallurgical bond of remelted coating and directional structure coating (wt%)

Main element	Fe	Ni	Cr	Cu	C	Si	Al	B	Co	Mn	O
Remelting coating	73.0	11.2	3.0	3.1	7.3	1.2	1.0	1.5	0.1	0.2	1.0
Directional structure coating	61.4	15.4	4.0	3.8	11.1	1.0	0.3	1.0	0.5	0.5	1.0

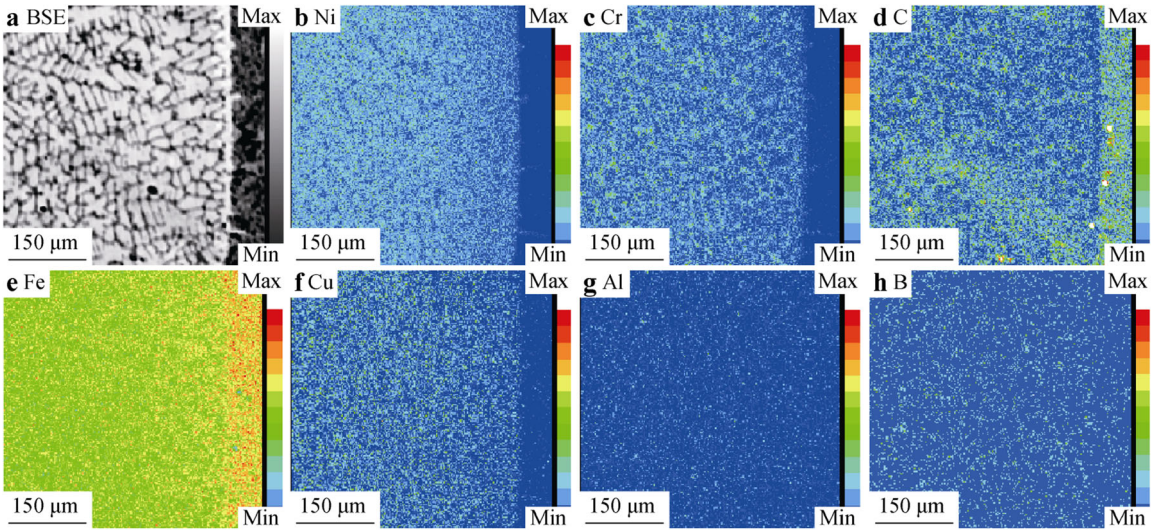

Fig. 3 **a** Backscattered electron (BSE) and corresponding EPMA maps for different elements (**b** Ni, **c** Cr, **d** C, **e** Fe, **f** Cu **g** Al and **h** B) of remelted coating cross section

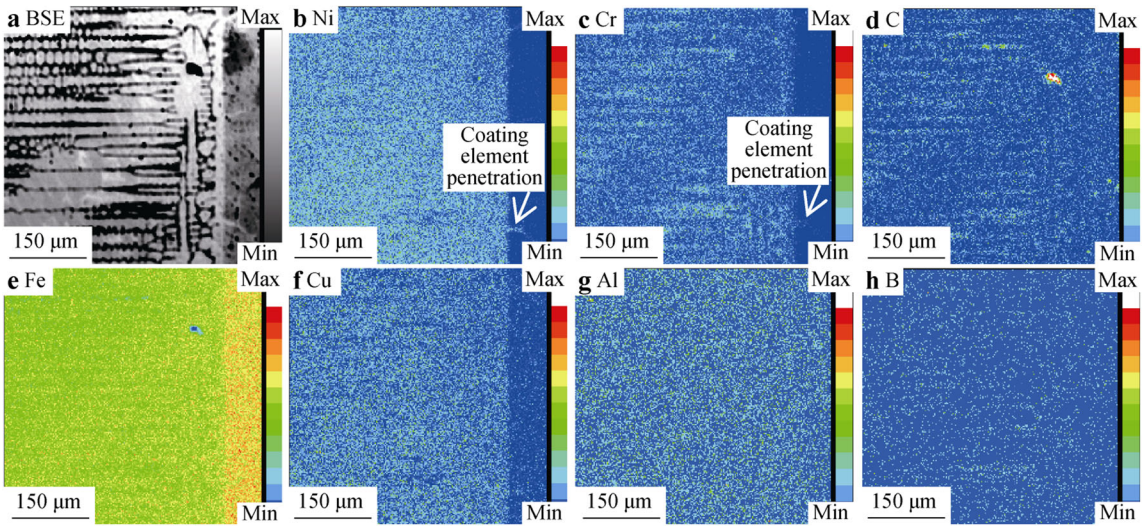

Fig. 4 **a** Backscattered electron (BSE) and corresponding EPMA maps for different elements (**b** Ni, **c** Cr, **d** C, **e** Fe, **f** Cu **g** Al and **h** B) of directional structure coating cross section

of the substrate elements of the remelted coating is more stronger than that of the directional structure coating due to rapid cooling.

EPMA maps (Figs. 3, 4) also show that Fe, Ni and Cu form the atom-rich zones in the crystal axis of both coatings, and Cr, C and B are rich in the crystal boundary. This is due to the fact that Fe and Cu preferentially form compounds or solid solutions with Ni during the solidification process, but Cr, C and B precipitate and wrap the crystal axis, forming grain boundary reinforcement phase. Therefore, the organization structure formed is tough inside and hard outside. For the forced cooling coating, it is like the trunk wrapped a hard bark, which will have an important influence on the mechanical properties and tribological properties of the coating. It makes the coating have low hardness, but good wear resistance because of enhanced ability of lateral shear [20].

Compared with forced cooling coatings, the remelted coating exhibits cross-shaped and granular equiaxed grains, which are disordered and larger near the substrate. This is because that the interface is in the melting state for the longer time, and grains have more time to grow up [21, 22].

Figure 2b shows the microstructure of coatings when the cooling rate is 0.943 $ml \cdot min^{-1} \cdot mm^{-2}$. The smaller temperature cannot provide sufficient conditions for the rapid solidification of the grains, which makes grains

possess a distinct coarser dendritic character. Moreover, the grains show competitive merger growth and competitive elimination mechanism and have rightward angles of 25° to 30° deviating from the heat flow direction, as shown in Fig. 2b1. The surface structures have the sheet character of the lateral expansion growth, as shown in Fig. 2b2.

Figure 2c shows the microstructure of coatings when the cooling rate is 1.415 ml·min^{-1}·mm^{-2}. The directional structure is more evident, the dendrites are significantly refined, and the dendritic spacing significantly reduces, as shown in Fig. 2c1. The stronger cooling rate suppresses the lateral extension of the secondary dendrite and makes the surface show a cross-shaped structure with regular alignment, as shown in Fig. 2c2. The grains of the longitudinal structure have divergent growth character, but the competition growth is not obvious, and the grains deviate from the heat flow direction to the left with the angle of $\alpha = 17°$ and to the right with the angle of $\theta = 23°$ (Fig. 2c1).

Figure 2d1 shows that the columnar cellular crystal structure is very distinct and grains can grow along the heat flow direction when cooling rate is 1.886 ml·min^{-1}·mm^{-2}. Under such circumstances, the initial grain orientation, temperature field, solute field and external environment have a good fitting relationship, which makes the grain grow linearly in a very steady state with a certain inclination by repeated adjustment of the dynamic equilibrium relationship [23–25]. Figure 2d2 shows the tiny cross-shaped and small equiaxed structure that is similar to that in Fig. 2c2, but the structure alignment is not so regular and neat, as shown in Fig. 2c2.

Figure 2e1 shows the "X-shaped" structure in longitudinal section of the coating, indicating that the grains of the preferential formation prevent the other grains from growing continuously when the cooling rate is 2.358 ml·min^{-1}·mm^{-2}. Thus, the grains show directional tendency on the whole, but the formation of directional structure is inhibited in the short distance. The result shows that the grains grow and merge (Circle 1 in Fig. 2e1), compete and are eliminated (Circle 2 in Fig. 2e1), converge and form new growth direction (Circle 3 in Fig. 2e1), and this process is repeated, but the grains are coarser compared with those in Fig. 2c2, d2, as shown in Fig. 2e2, which is thought to be that the overlarge cooling rate does not provide stable growth interface but rather promotes competition and merge of grains.

On the whole, with the increase in the cooling rate, the structure transformation is as follows: dendrite → cellular dendrite with directional orientation → fine cellular dendrite with directional orientation → dendrite. But it can be regarded that the directional structure is not easy to form in the coatings under too low or high cooling rate.

3.2 The micro-interface morphology

Figure 5 shows the micro-interface morphology of forced cooling coating and remelted coating. The grain boundary of forced cooling coating is smooth due to rapid solidification of the melts, forming a nanoscale symbiotic eutectic band at the edge of the matrix phase (as marked in Fig. 5a), which obstructs continuous precipitation of matrix composition. Simply considering the temperature and ignoring constitutional undercooling, the planar growth condition equation is as follows [26]:

$$\frac{G_L}{R} \geq \frac{m_L C_0 (1-k)}{D_L k} \tag{1}$$

where G_L is the temperature gradient, R is the velocity of growth, m_L is the slope of the liquidus, C_0 is the initial alloy composition, k is solute partition coefficient, and D_L is solute diffusion coefficient. Under forced cooling condition, there is a larger temperature gradient (G_L) at the interface front. The velocity of growth can be generally expressed as [26]:

$$R = \frac{G_S \lambda_S - G_L \lambda_L}{\rho L} \tag{2}$$

where R is the velocity of growth, G_L and G_S are temperature gradients in the liquid and solid phase, respectively, λ_S and λ_L are thermal conductivities of crystals and melts, respectively, ρ is melt density near the melting point, and L is crystallization latent heat released by unit mass of crystals.

The increase in the temperature gradient inevitably makes the growth velocity decrease, which provides conditions for regular symbiotic eutectic growth of non-faceted–non-faceted planes; according to the actual solidification conditions, this organization should be a pseudo-eutectic organization.

In the wider region of the crystal boundary, the precipitates reach dynamic equilibrium and form lamellar and granular eutectic structure, which also belongs to the non-faceted–non-faceted regular eutectic growth character, as marked by A in Fig. 5a and shown in Fig. 5b. The solute phases that remain in the matrix are solidified rapidly and become strengthening phases, showing white dots or distributed spherules (as marked by B in Fig. 5a). Combined with the preparation process of the coating, it can be regarded that the main branch of the grains has higher heat conductivity coefficient than the crystal boundary, which results in the main branch being undercooling untimely; thus, a lateral temperature gradient is formed between the main branch phase and crystal boundary. The lateral temperature gradient affects interface morphology, solute diffusion, phase composition and the size of grain boundary.

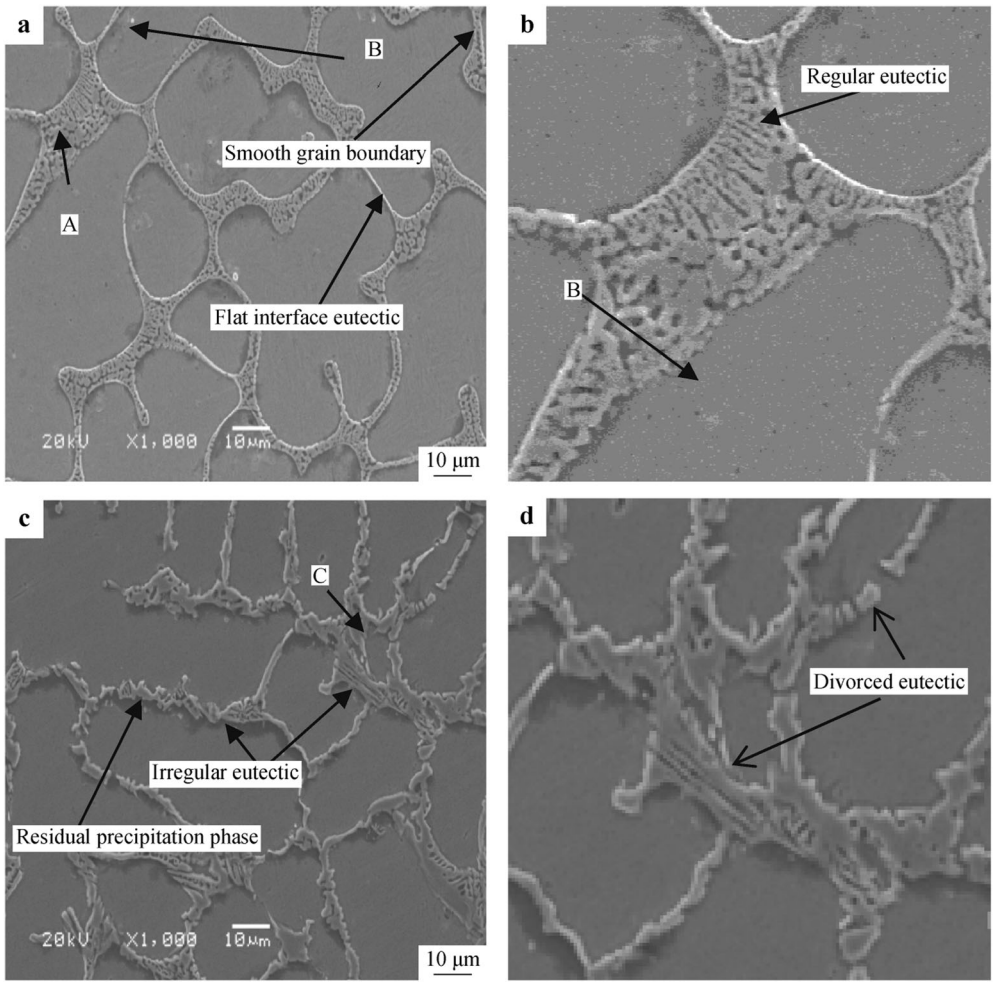

Fig. 5 Micro-interface SEM images: **a** directional structure coating, **b** partial enlarged detail of **a**, **c** remelted coating and **d** partial enlarged detail marked in **c**

However, the grain boundary of remelted coatings exhibits rough divorced eutectic character with non-faceted–faceted irregular structure (Fig. 5c), which is non-symbiotic eutectic microstructure and Widmanstatten structure (as marked by C in Fig. 5a and shown in Fig. 5d). There are a little bit of solute phases remaining near the grain boundary, but there are few in middle part of the matrix phase (marked in Fig. 5c, d), which is due to that the precipitation phases do not completely reach the grain boundary in precipitation process and aggregate in the form of small particles near the grain boundary during the solidification.

The content of precipitates and their distribution in the coatings were analyzed by using Image-Pro Plus 6.0. To obtain more detailed information and more accurate results, the micrographs with different magnifications are taken, and the average values of multiple specimens are counted. The percentage of precipitates and their average value of different magnifications are given in Table 4. It indicates that the remelted coating has higher precipitate content than the directional structure coating, due to that forced cooling inhibits the precipitation of solute elements, which is identical with the interface growth theory previously discussed.

Table 4 Content of precipitates of remelted coating and directional structure coating (vol%)

Magnification	100				500				1000				Average value
Remelting coating	1.43	8.94	7.32	6.31	3.64	7.05	6.07	8.79	5.61	9.58	7.14	10.63	6.61
Directional structure coating	0.77	2.5	6.86	7.3	3.01	7.94	6.74	6.33	4.36	8.93	7.27	9.12	5.78

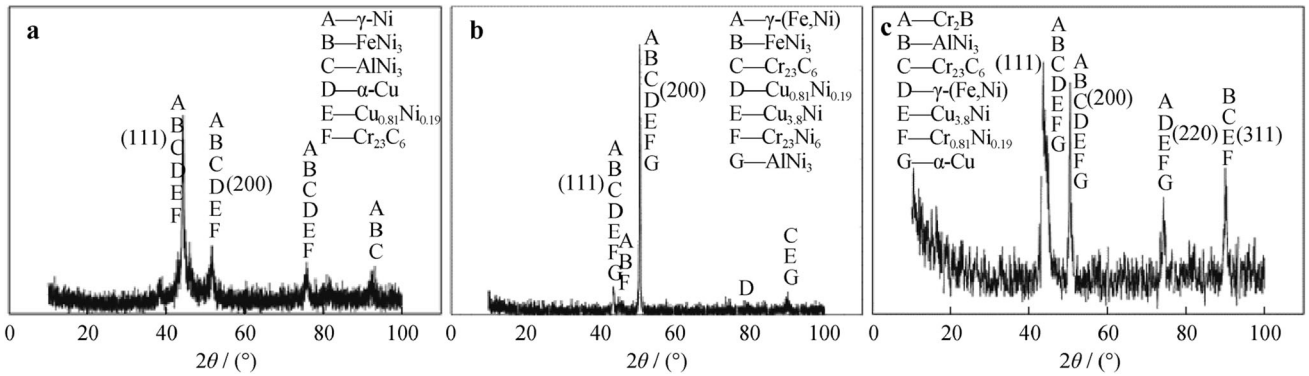

Fig. 6 XRD patterns of coating surface: **a** as-sprayed coating, **b** remelted coating and **c** directional structure coating

3.3 Phase analysis

XRD patterns of the coatings are depicted in Fig. 6. It is notable that the γ-(Fe, Ni) and $Cu_{3.8}Ni$ phases form in the remelted coating and directional structure coating compared with as-sprayed coating due to the redistribution of elements, but there is no evident difference between directional structure coating and remelted coating. Combined with the distribution of elements discussed above, it can be concluded that the equiaxed crystal, plane crystal and dendrite crystal are all mainly composed of the solid solution with Ni, Fe and $Cu_{3.8}Ni$ compounds, and they are surrounded by $Cr_{23}C_6$ and Cr_2B phases which play a significant role in intergranular strengthening [27, 28]. The $Cu_{0.81}Ni_{0.19}$ phase is transferred into $Cu_{3.8}Ni$ phase at high temperature [29]. The α phase in the three kinds of coatings is the Cu-based solid solution with face-centered lattices. The α phase is ductile, which can not only support and connect the hard phases, but also disperse the stress sustained by the hard phase, to some extent; it has an important role in the densification of the organization and the anti-friction property [30].

Also, the peak shape and diffraction angle have significant differences in three kinds of coatings. The as-sprayed coating shows the diffused peak shape and the main peak at 44°. The remelted coating exhibits relatively stable peak shape and stronger peak intensity at 52°. The significant reduction in half-peak breadth indicates obvious crystallization tendency and larger grain size from Scherrer formula. The main peak position shifts to a large angle, which implies smaller interplanar spacing according to Bragg equation. Figure 6c presents hybridized peak shape and multiple main peaks with broadening phenomena. Not only the diffuse main peaks appear at 44° and 52°, but also some appear in larger angles, which implies there is the amorphous tendency in condition of forced cooling, and the structure of different interplanar spacing is formed.

Compared with the (111) preferred orientation of the as-sprayed coating, (200) plane is the preferred orientation in the remelted coating. However, the (111) and (200) planes all have strong growth orientation in directional structure coating, indicating that there is fierce competition in the grain growth.

3.4 Wear resistance

The weight loss of the coatings under the loads of 50 and 150 N and with test duration of 10 min is shown in Fig. 7. It can be seen that the weight loss of three kinds of coatings under the load of 50 N is lower than that under 150 N. Under the condition of the same load, the weight loss of the remelted coating and directional structure coating was much lower than that of the as-sprayed coating, and the weight loss of directional structure coating is lower than that of the remelted coating, as shown in Fig. 7. The result indicates that directional structure coating has the best wear resistance among the three kinds of coatings. It may be attributed to the elimination of defects, the reduced porosity and the micro-cracks during induction remelting. In addition, the forced cooling makes the coating solidify rapidly and form the directional structure, which eliminates the transverse grain boundaries. Thus, the wear resistance of directional structure coating is greatly enhanced.

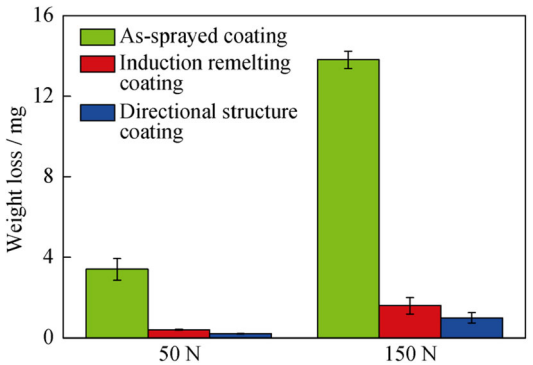

Fig. 7 Weight losses of coatings under loads of 50 and 150 N and test duration of 10 min

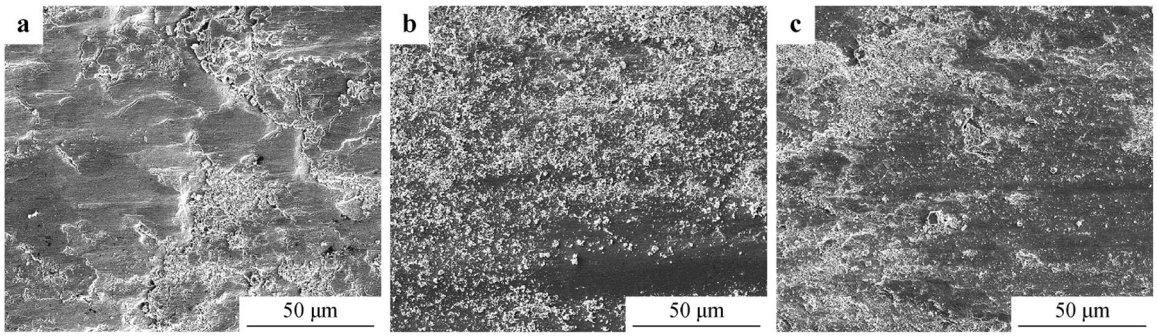

Fig. 8 Wear SEM images of different structure-orientation coatings under 150 N: **a** as-sprayed coating, **b** induction remelting coating and **c** directional structure coating

The worn surface morphology of different structure-orientation coatings under 150 N observed by SEM is shown in Fig. 8. The wear track and fatigue cracking can be observed on the worn surface of the as-sprayed coatings due to stripping along grain boundaries between layers. Many tiny abrasive particles are attached on the worn surface of the remelted coatings, and the main wear mechanism is a mild regime of smear and adhesive wear. A handful of wear debris adhered to the surface of the directional structure coating during the friction process, and the wear debris would continue to accumulate. It can be attributed to the migration of the stripping materials and the effect of directional structure orientation.

4 Conclusion

In this study, the structure, interface, distribution of element, grain boundary and phase composition of remelted coating and forced cooling coating have been investigated. Experimental results show that the metallurgical bonding is formed in forced cooling coating and remelted coating. The coating elements diffuse along the grain boundary of substrate and form the pinning effect, but forced cooling makes the diffusion more stronger and forms wrapped-pinning in substrate. The microstructures of grains wrapped by crystal boundary precipitation $Cr_{23}C_6$ and Cr_2B, etc., are formed, and the microstructures are transferred from directional dendrite crystal to cellular dendrite with directional orientation, fine cellular dendrite with directional orientation, and then to directional dendrite crystal again with the increment of the rate of cooling, but overlarge cooling rate is adverse to forming directional crystals.

Remelted coating has the evident crystallization phenomenon and the (111) preferred orientation. However, the directional structure coating has (111) and (200) preferred orientations and has diffraction peak differentiation and broadening phenomenon. The directional structure coating has the best wear resistance compared to remelted coating and as-sprayed coating.

Acknowledgements This study was financially supported by the National Natural Science Foundation of China (No. 51365024) and Zhejiang Provincial Natural Science Foundation of China (No. LGG19E010003).

References

[1] He L, Tan YF, Tan H, Tu YQ, Zhang ZW. Microstructure and tribological properties of WC-CeO_2/Ni-base alloy composite coatings. Rare Met Mater Eng. 2014;43(4):823.
[2] Wang X, Zhu LF, Zhou ZM, Liu G, Liu EY, Zeng ZX, Wu XD. Tribological properties of WC-reinforced Ni-based coatings under different lubricating conditions. J Therm Spray Technol. 2015;24(4):1323.
[3] Hu ZL, Pang Q, Ji GQ, Wu GH. Mechanical behaviors and energy absorption properties of Y/Cr and Ce/Cr coated open-cell nickel-based alloy foams. Rare Met. 2018;37(8):650.
[4] Jin H, Wang YY, Wang YT, Yang HB. Synthesis and properties of electrodeposited Ni-CeO_2 nano-composite coatings. Rare Met. 2018;37(2):148.
[5] Bai MW, Song B, Reddy L, Hussain T. Preparation of MCrAlY-Al_2O_3 composite coatings with enhanced oxidation resistance through a novel powder manufacturing process. J Therm Spray Technol. 2019;28(3):433.
[6] Luo WY, Liu YZ, Luo Y, Wu M. Fabrication and characterization of WC-AlCoCrCuFeNi high-entropy alloy composites by spark plasma sintering. J Alloys Compd. 2018;754:163.
[7] Zhang YY, Brodusch N, Descartes S, Shockley JM, Gauvin R, Chromik RR. The effect of submicron second-phase particles on the rate of grain refinement in a copper-oxygen alloy during cold spray. J Therm Spray Technol. 2017;26(7):1509.
[8] Huang K, Marthinsen K, Zhao Q, Logé RE. The double-edge effect of second-phase particles on the recrystallization behaviour and associated mechanical properties of metallic materials. Prog Mater Sci. 2018;92:284.
[9] Gao Y, Luo BH, Jing HB, Chen W, Bai ZH, Zhang WW. Vacuum sintering of WC-Fe-Ni-Co cemented carbides. Chin J Rare Met. 2018;42(5):477.
[10] Alam S, Sasaki S, Shimura H. Friction and wear characteristics of aluminum bronze coatings on steel substrates sprayed by a low pressure plasma technique. Wear. 2001;248(1–2):75.

[11] Li WS, Wang ZP, Lu Y, Yuan LH, Xiao RZ, Zhao XD. Corrosion and wear behaviors of Al-bronzes in 5.0% H_2SO_4 solution. Trans Nonferrous Met Soc China. 2009;19(2):311.
[12] Yang X, Li X, Yang X, Lu Y, Wang P, Li W. Preparation of multivariate multiphase composite coating of Ni60/high aluminum bronze and its microstructure characteristics. J Harbin Eng Univ. 2016;37(3):461.
[13] Glicksman ME. Handbook of Crystal Growth. Edited by Nishinaga T. Boston: Elsevier B.V. 2015. 669.
[14] Qu M, Liu L, Cui Y, Liu FB. Interfacial morphology evolution in directionally solidified Al-15% Cu alloy. Trans Nonferrous Met Soc China. 2015;25(2):405.
[15] Yang C, Xu QY, Liu BC. Primary dendrite spacing selection during directional solidification of multicomponent nickel-based superalloy: multiphase-field study. J Mater Sci. 2018;53(13):9755.
[16] Liu H, Xuan WD, Xie XL, Yu JB, Wang J, Li X, Zhong YB, Ren ZM, Wang H, Dai YM. Effect of a high magnetic field on solidification structure in directionally solidified NiAl-Cr(-Mo)-Hf eutectic alloy. J Alloys Compd. 2018;737:74.
[17] Yang XC, Li GL, Wang HD, Dong TS, Kang JJ. Effect of flame remelting on microstructure and wear behaviour of plasma sprayed NiCrBSi-30%Mo coating. Surf Eng. 2016;34(3):181.
[18] Dong TS, Liu L, Li GL, Wang R, Yuan JM, Feng Y. Effect of induction remelting on microstructure and wear resistance of plasma sprayed NiCrBSiNb coatings. Surf Coat Technol. 2019;364:347.
[19] Lu Y, Ma JZ, Yang XT, Xiao RZ, Yang XW. Investigation of organization structure optimized by Ni60 on high-aluminum copper alloy coating prepared by supersonic plasma spraying-induction remelting. J Fun Mater. 2014;45(7):7108.
[20] Yang XT, Wang PC, Li X, Lu Y, Xiao RZ. Evolution characteristic of microstructure of Ni-based alloy coatings and their properties under complex process. Rare Met Mater Eng. 2017;46(3):693.
[21] Liang B, Zhang Z, Guo H. Comparison on the microstructure and wear behaviour of flame sprayed Ni-based alloy coatings remelted by flame and induction. Trans Indian Inst Met. 2016;70(7):1.
[22] Schmelzer JWP, Abyzov AS. How do crystals nucleate and grow: Ostwald's rule of stages and beyond. In: Šesták J, Hubík P, Mareš J, editors. Thermal Physics and Thermal Analysis. Switzerland: Springer; 2017. 195.
[23] McLean M. Directionally solidified materials for high temperature service. Br Corros J. 1984;19(4):154.
[24] Huang XR, Han ZQ, Liu BC. Study on the effect of pressure on the equilibrium and stability of the solid-liquid interface in solidification of binary alloys. Sci China Technol Sci. 2011;54(2):479.
[25] Liu L, Hang TW, Zhang J, Fu HZ. Microstructure and stress rupture properties of single crystal superalloy CMSX-2 under high thermal gradient directional solidification. Mater Let. 2007;61(1):227.
[26] Hu HQ. Principle of Metal Solidification. Beijing: China Machine Press; 2000. 13.
[27] Gao Y, Wang CL, Huang JQ, Huang XF. Microstructure and wear resistance of Ni60 layer prepared by high-frequency induction cladding. Rare Met Mater Eng. 2011;40(S2):309.
[28] Chen YD, Zheng WW, Zheng YR, Feng Q. Microstructural evolution and corresponding stress rupture property in DZ125 alloy after thermal exposure. Chin J Rare Met. 2018;42(10):1009.
[29] Liu XZ, Shen QW, Liu XZ, Chen J, Zhu LW, Qi J. Effect of heat treatment temperature on the spectral properties of Cu-Ni coating. Spectrosc Spec Anal. 2015;35(4):1094.
[30] Yang XT, Wang ZP, Lu Y, Li WS, Li X, Liu JZ. Characteristics of high-aluminium copper alloy coating made by supersonic plasma spraying and induction refusion composite technology. J Harbin Eng Univ. 2012;33(7):906.